Geoelectric structures modelling around unconformity-related uranium deposits through joint inversion of electromagnetic and electrical data.

A. Mohand-said[1], G. Marquis[1], S. Sambolian[1], J. Girard[1], G. Harrison[2], E. Williard[3]

[1] Universite de Strabourg - CNRS - ITES; [2] Orano Canada Inc.; [3] Orano Mining

Summary

Exploration of Uranium deposits in the Athabasca Basin relies on localizing graphitic conductors and alteration halos, as they are closely related to mineralization, using electromagnetic and electrical methods. To evaluate the benefits of joint inversion of electromagnetic and electrical data we inverted a dataset composed of coincident time-domain electromagnetic moving-loop and pole-dipole electrical resistivity surveys. Standalone inversion of electromagnetic data succeeds in identifying the graphitic conductors, while standalone inversion of electrical data reveals a single horizontal conductive body below the expected depth of unconformity. Models obtained by standalone inversions of a single dataset do not fit the data from the other. Joint inversion of the two datasets produces a single geoelectric model that fits both datasets. The model obtained shows the graphitic conductors identified on electromagnetic inversion and reveals resistivity contrasts not seen in the standalone inversions.

Geoelectric structures modelling around unconformity-related uranium deposits through joint inversion of electromagnetic and electrical data.

Introduction

The Athabasca Basin (Saskatchewan, Canada) hosts some of the world's best-known high-grade, high-tonnage uranium deposits. Current metallogenic models link ore formation to fluid-rock interactions at the unconformity between the basement metamorphic and plutonic rocks, and the overlying sediments, essentially sandstone. Hydrothermal fluid flow in the basement is driven through deep-rooted faults and shear zones where graphite gets deposited (Jefferson et al. (2007)).
Both basin and basement rocks are highly resistive, typically several thousands of $\Omega.m$, while graphitic structures are highly conductive. Inductive electromagnetic methods are well-suited to locate these high resistivity contrasts and are therefore first-order tools for uranium exploration projects in the Athabasca (Powell et al. (2007), Nimeck and Koch (2008)).
Fluid flow leading to uranium mineralization also produces a significant alteration of the clay of the surrounding sandstones and results in a decrease in resistivity, down to a few hundred $\Omega.m$. Alteration markers associated with graphitic structures are therefore indicative of massive fluid flows, allowing precipitation of proportionally larger ore volumes. Such association is thus a priority target in exploration project of uranium deposits in Athabasca. However, altered rocks are not conductive enough to provoke a strong inductive response. Electrical resistivity methods are better suited to detect the mild resistivity contrasts associated with alteration (Powell et al. (2007), Legault et al. (2008)).
Electromagnetic and electrical methods are, thus, both sensitive to electrical resistivity but highlight different geoelectric structures. Standard strategies for inversions of electromagnetic and electrical data usually do not attempt to take advantage of their respective sensitivities. Separate inversions of electrical and electromagnetic data often yield geoelectric models that do not satisfy both datasets.
We are here evaluating the benefits from 2D joint inversion of electromagnetic and electrical resistivity data around unconformity-related uranium deposits by comparing them to standalone inversion results. We illustrate our approach with a case study on ground moving-loop time-domain electromagnetic and pole-dipole direct-current resistivity data acquired over coincident lines, at the Waterbury-Cigar Lake area in the eastern Athabasca Basin.

Method

Modelling

Maxwell's equations describe the relationship between electric and magnetic fields and constitute the basis for formulating time-domain electromagnetic and direct-current resistivity problems.
For the time-domain electromagnetic problem, a quasi-static approximation of Maxwell's equation is used to model electromagnetic fields. The secondary magnetic field $\mathbf{B}$ induced by a magnetic source $\mathbf{B}_s$ is given by

$$-\frac{1}{\mu_0}\nabla^2\mathbf{B}+\sigma\frac{\partial\mathbf{B}}{\partial t}=\sigma\frac{\partial\mathbf{B}_s}{\partial t} \tag{1}$$

with μ_0 the magnetic permeability of free space, and t the time.
For the direct-current resistivity problem, the steady-state Maxwell's equations associate a source current density ($\mathbf{j}_s$) to an electric potential ($\mathbf{V}$) via the electrical conductivity σ:

$$\nabla\cdot(\sigma\nabla\mathbf{V})=\nabla\mathbf{j}_s \tag{2}$$

Numerical solutions of these sets of equations, discretising the problems on tensor meshses, were obtained using the finite-volume approach implemented in the SimPEG open-source codes (Cockett et al. (2015), Heagy et al. (2017)).
Modelling of electric potential for the DC resistivity problem uses a 2.5D approximation, considering a 2D resistivity model and a 3D source. For the time-domain electromagnetic problem, the resistivity model was defined on a 2D grid then mapped on a 3D grid for computation of B-field, considering uniform electrical resistivity in the direction perpendicular to the model. For both problems the same 2D resistivity model is used.

Inversion

The inverse problem is addressed as a data-fitting problem minimizing the squared L2-Norm of the difference between the observed $\mathbf{d}_{obs}$ and predicted data $\mathbf{d}_{pred}$, weighted by $\mathbf{W}_d$, a diagonal matrix containing the reciprocal of data errors,

$$\Phi = \frac{1}{2}||\mathbf{W}_d(\mathbf{d}_{pred} - \mathbf{d}_{obs})||_2^2 \tag{3}$$

The problem is solved iteratively using a Gauss-Newton trust-region method (Conn et al. (2000), Nocedal and Wright (2006)). Trust-region globalization strategy allows to get implicit regularization of the problem by limiting the size of the model perturbation to the trust-region radius (Δ_i). The trust-region size is adapted over iterations depending on the misfit decrease obtained with the computed perturbation p_i and the expected misfit based on the local quadratic approximation of the cost function built around the model x_i. The more accurate is the quadratic approximation, the more the trust-region can be expanded. At each iteration the problem solve is given by (3), with $\mathbf{J}$ the jacobian matrix, and Φ' the gradient of the cost function Φ.

$$\mathbf{p}_i(\mu) = -(\mathbf{J}(\mathbf{x}_i)^T\mathbf{W}_d^T\mathbf{W}_d\mathbf{J}(\mathbf{x}_i)) + \mu\mathbf{M})^{-1}\Phi'(\mathbf{x}_i) \tag{4}$$

given the following constraint:

$$\mu(||\mathbf{p}_i(\mu)||_{\mathbf{M}} - \Delta_i) = 0 \tag{5}$$

$\mathbf{M}$ being a symmetric positive-definite matrix. Starting with the full Gauss-Newton step, $\mu = 0$, μ is progressively increased until the constraint is satisfied. Here $\mathbf{M}$ is chosen as an approximation of the discrete Laplacian operator of the model, to constraint the roughness of the model. Thus at each iteration the roughness of the model is adapted to allow global convergence of the inversion.

Data

We selected two data sets from a single coincident profile perpendicular to one of the main magnetic trends in the vicinity of the Cigar Lake mine, in the eastern part of the Athabasca Basin.
The first is a moving-loop, time-domain electromagnetic survey using a single-turn $400 \times 400\text{m}^2$ loop, excited by a bipolar square wave signal of 23.5 A with a base frequency of 5 Hz. Measurements of the three components of the secondary B-field were made in a Slingram configuration with the receiver positioned 800 m from the transmitter and with a station spacing of a 100 m, over 29 geometrically-spaced time gates ranging from 0.10 ms to 42.68 ms off-time. The second is a DC resistivity survey using a pole-dipole array with a dipole length of 100 m. A maximum of 60 n levels were recorded, ranging from $n = 0.5$ to $n = 59.5$.
To reduce the computational cost, we limited the moving-loop data to 26 stations spaced 200 m apart from X=-2500 m to X=2500 m. We inverted only the vertical component of the 15 earliest time gates, 0.10 to 2.07 ms (Figure 1B. We restricted the direct-current resistivity data to quadrupoles with a geometric factor lesser or equal to 100000 (Figure 1A).

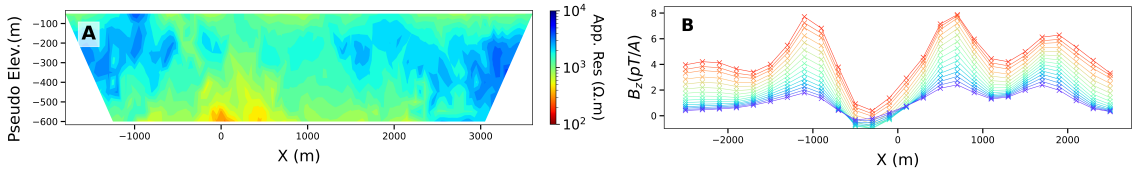

Figure 1 *Resampled field data (A) Pseudo-section of apparent resistivity; (B) Moving-loop EM profile, red lines and dots corresponds to earliest time channels, and blue ones to the latest time channels.*

Results

Separate electromagnetic and electrical inversions, as well as a joint inversion are run for all models. For all inversions, the discretization and algorithm remain the same. Starting models for the inversions

are 1000 Ω.*m* halfspaces. Inversions are run for up to 29 iterations or until the radius of the trust-region reaches a predefined lower limit, set at a fraction of the initial value. After 29 iterations, the RMS decreased to 1.067, 1.162, 1.08 for electromagnetic-only, electrical-only and joint inversion respectively. To get comparable results, we retained the first inversion model reaching a threshold RMS value of 1.2 for each inversion.

For the electrical-only inversion, the main feature is a broad conductive anomaly between X=-1000 m and X=2700 m, with a top close to 400 m underlying resistive layers (Figure 2A). The core of this body is located at X=0 m with a resistivity of 20 Ω.*m*. This large anomaly underlies a resistive layer of a few thousand Ω.*m* that almost reaches the surface. Even shallower, a near-surface layer, of about 50 m thickness, i.e. the minimum cell size, of a few hundred Ω.*m*, to a thousand Ω.*m* is modeled. Several lateral discontinuities cut this top layer that could be attributed to lakes, surface geology, or topography variations. As an exercise, moving-loop time-domain electromagnetic data were calculated for this resistivity model and they show a very large misfit with the measured data with an RMS error of 35.285.

The EM-only inversion yields five distinct subvertical conductive anomalies embedded in a resistivity background of a few thousand Ω.*m* (Figure 2B). The leftmost anomaly is centered on X=-2000 m, and has a resistivity of 100 Ω.*m* to 200 Ω.*m*. Two bodies centered at X=-500 m and X=0 m of few Ω.*m* seem to be connected but do not have much depth extent nor a dipping trend. Their tops are at abut 350 m depth. The fourth conductor centered on X=1400 m is slightly less conductive with a resistivity of 20 Ω.*m* but shows a steep dip to the north . This body has its top at 450 m to 500 m depth. The rightmost anomaly is centered at X=2500 m. Its top is at about 450 m and its resistivity is 10 Ω.*m*. The tops of all the conductors recovered with standalone EM inversion is consistent with the expected depth of unconformity, their conductivities contrast sharply with their background and they show significant vertical extent. This result is consistent with our geological knowledge of the area. Again as a comparison, electrical resistivity data calculated on this resistivity model are very different from the observed data with an RMS error of 38.974.

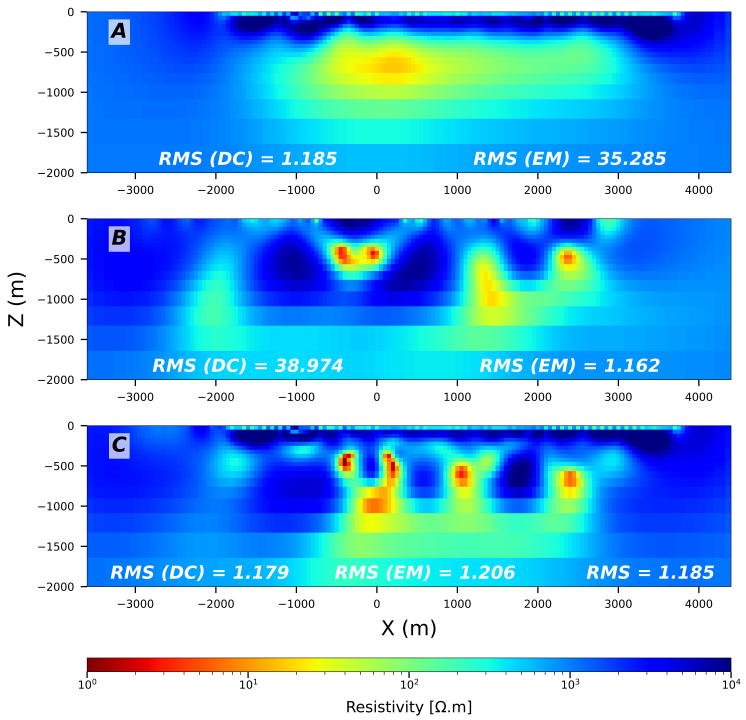

Figure 2 *Inverse models of Athabasca basin field data (A) Standalone electrical inversion; (B) Standalone electromagnetic inversion; (C) electrical and electromagnetic joint inversion.*

On the joint inversion results, the conductors identified on the EM-only inversion and the layered structure identified on the resistivity-only inversion are all recovered with slight changes (Figure 2C). The leftmost conductive anomaly is however weaker and its interpretation as a strong conductor can be

discarded. Other conductive anomalies are showing variations in lateral position as well as dip. The conductor centered at X=1400 m on the EM-only inversion is now centered on X=1050 m. Two conductive anomalies dipping in opposite directions but rooted to a deeper conductive body not identified on the EM-only inversion come out clearly on joint inversion. Their resistivities range from a few tens to a few hundred $\Omega.m$ and their tops are at 300 m depth. Their resistivity values, positions and geometry strongly suggest occurrences of alteration, particularly for the north-dipping conductor. The geoelectric model obtained by joint inversion reconciles both electromagnetic and electrical measurements, RMS errors are respectively 1.206 (Figure 2C) and 1.179 (Figure 2C).

Conclusions

This work aimed to assess the outcome of 2D joint inversion of electrical and electromagnetic data from the eastern part of the Athabasca Basin. We show that both EM-only and electrical-only inversions, although both bring insights on the subsurface resistivity, fail to produce models that satisfy both datasets. The model obtained by joint inversion however fits very well both datasets and show all the conductors identified on EM-only inversion and the layered resistive background identified on electrical-only inversion. Including information from near-surface structures leads to variations of structural orientations of conductive plates. In addition, better-focused subsurface conductors allows resolution of weaker overlying conductivity contrasts, potentially related to alteration.

Acknowledgements

This research is supported by the GeoMin3D Industrial Chair (PI Dr. Julien Mercadier, Géoressources Nancy) funded by Orano and ANR. We are grateful for their involvement in the project. Our acknowledgements go to Cameco and Orano for providing us with the Cigar Lake data. We also acknowledge our colleague Alessandro Vinciguerra for fruitful discussions. The authors would like to acknowledge the High Performance Computing Center of the University of Strasbourg for supporting this work by providing scientific support and access to computing resources. Part of the computing resources were funded by the Equipex Equip@Meso project (Programme Investissements d'Avenir) and the CPER Alsacalcul/Big Data.

References

Cockett, R., Kang, S., Heagy, L., Pidlisecky, A. and Oldenburg, D. [2015] SimPEG: An open source framework for simulation and gradient based parameter estimation in geophysical applications. *Computers and Geosciences*, **85**, 142–154.

Conn, A., Gould, N. and Toint, P. [2000] *Trust Region Methods*. Society for Industrial and Applied Mathematics.

Heagy, L., Cockett, R., Kang, S., Rosenkjaer, G. and Oldenburg, D. [2017] A framework for simulation and inversion in electromagnetics. *Computers and Geosciences*, **107**, 1–19.

Jefferson, C.J.W., Thomas, D.J., Gandhi, S.S., Ramaekers, P., Delaney, G.D., Brisbin, D., Cutts, C.J., Portella, P. and Olson, R.A. [2007] Unconformity-associated uranium deposits of the Athabasca Basin, Saskatchewan and Alberta. In: Goodfellow, W. (Ed.) *Mineral Deposits of Canada: A Synthesis of Major Deposit-Types, District Metallogeny, the Evolution of Geological Provinces, and Exploration Methods*. Geological Association of Canada, 273–305.

Legault, J., Carriere, D. and Petrie, L. [2008] Synthetic model testing and distributed acquisition dc resistivity results over an unconformity uranium target from the Athabasca Basin, northern Saskatchewan. *The Leading Edge*, **27**, 46–51.

Nimeck, G. and Koch, R. [2008] A progressive geophysical exploration strategy at the Shea Creek uranium deposit. *The Leading Edge*, **27**, 52–63.

Nocedal, J. and Wright, S. [2006] *Numerical Optimization*. Springer New York.

Powell, B., Wood, G. and Bzdel, L. [2007] Advances in Geophysical Exploration for Uranium Deposits in the Athabasca Basin. In: Milkereit, B. (Ed.) *Proceedings of Exploration 07: Fifth Decennial International Conference on Mineral Exploration*. 771–790.